# Supplementary Material: On the drivers of Mediterranean Marine Cold Spells under Climate Change

Sofia Darmarak[1], Marco Reale[2], Robin Waldman[3] , Vassiliki Metheniti[1],

[1]Foundation for Research and Technology, Hellas (FORTH),

[2]National Institute of Oceanography and Applied Geophysics-OGS, Trieste, Italy

[3]Météo-France, CNRS, Univ. Toulouse, CNRM, Toulouse, France

*Correspondence to*: Sofia Darmaraki (sofia.darm@email.com)

**Table S1:** Simulation periods of CNRM-RCSM6 are shown for past and future MCSs (top row), using both fixed and moving baseline climatologies (bottom row). In the case of shifted climatologies, the moving reference windows are aligned with the corresponding simulation periods. Calculation of corresponding MLHB term anomalies were based on the same climatological baselines.

| **Simulation period** | **Hindcast** | **Historical** | **SSP5-8.5 GWL1** | | **SSP5-8.5 GWL2** | | **SSP5-8.5 GWL3** | | **SSP5-8.5 GWL4** | |
|---|---|---|---|---|---|---|---|---|---|---|
| **CNRM-RCSM6** | **1982-2014 ERA-Interim** | 1980-2014 | 2007-2026 | | 2036-2055 | | 2055-2074 | | 2070-2089 | |
| **Reference period** | **Fixed** | Fixed | Fixed | Moving | Fixed | Moving | Fixed | Moving | Fixed | Moving |
| | **1982-2014** | 1982-2014 | 1982-2014 | 2007-2026 | 1982-2014 | 2036-2055 | 1982-2014 | 2055-2074 | 1982-2014 | 2070-2089 |

**Table S2:** Basin-mean total MCS count, duration and intensity based on SST from the observations (1982-2014), the CNRM-RCSM6 hindcast run (1982–2014) and the CNRM-RCSM6 historical run (1982–2014).

| **Dataset** | **MCS property** | **Winter** | **Spring** | **Summer** | **Autumn** |
|---|---|---|---|---|---|
| **Satellite** | **MCS count (events)** | 12 | 14 | 11 | 12 |
| | **Duration (days)** | 14 | 13 | 11 | 14 |
| | **Intensity (°C)** | -1.3 | -1.7 | -2.1 | -1.8 |
| **CNRM-RCSM6 hindcast run** | **MCS count (events)** | 14 | 18 | 15 | 15 |
| | **Duration (days)** | 20 | 12 | 10 | 18 |
| | **Intensity (°C)** | -1 | -1.5 | -2 | -1.6 |

| | | | | | |
|---|---|---|---|---|---|
| **CRNM-RCSM6 historical run** | **MCS count (events)** | 14 | 17 | 17 | 16 |
| | **Duration (days)** | 21 | 12 | 10 | 17 |
| | **Intensity (°C)** | -1.2 | -1.6 | -2 | -1.7 |

**Table S3:** Pearson correlation coefficients and spatial RMSE between mean MCS duration patterns for (a) satellite vs. historical and hindcast simulations and (b) CNRM-RCSM6 hindcast vs. historical simulations, shown by season. MCSs were detected by applying Hobday et al. (2016) to SST. MCS durations are averaged over 1982–2014. Seasons are assigned based on MCS onset, irrespective of event termination.

| **Model Name** | **Index** | **Winter** | **Spring** | **Summer** | **Autumn** |
|---|---|---|---|---|---|
| **a)Comparison with Satellite data (1982-2014)** | | | | | |
| **CNRM-RCSM6 (HIND)** | **Corr.Coeff** | 0.2 | 0.1 | 0.3 | 0.09 |
| | **RMSE (days)** | 10.4 | 3.3 | 4 | 7 |
| **CNRM-RCSM6 (HIST)** | **Corr.Coeff** | 0.004 | -0.049 | 0.159 | 0.015 |
| | **RMSE (days)** | 11.3 | 3.8 | 3.7 | 6.9 |
| **b)Comparison with CNRM - RCSM6 Hindcast Run (1982-2014)** | | | | | |
| **CNRM-RCSM6 (HIST)** | **Corr.Coeff** | 0.3 | 0.3 | 0.4 | 0.3 |
| | **RMSE (days)** | 8.2 | 3.1 | 3.1 | 6.3 |

**Table S4**: As in Table S3 but for mean intensity patterns of historical surface MCSs.

| Model Name | Index | Winter | Spring | Summer | Autumn |
|---|---|---|---|---|---|
| **a) Comparison with Satellite data (1982-2014)** | | | | | |
| **CNRM-RCSM6 (HIND)** | **Corr.Coeff** | 0.50 | 0.51 | 0.73 | 0.70 |
| | **RMSE (days)** | 0.39 | 0.29 | 0.34 | 0.32 |
| **CNRM-RCSM6 (HIST)** | **Corr.Coeff** | 0.31 | 0.35 | 0.74 | 0.62 |
| | **RMSE (days)** | 0.31 | 0.27 | 0.35 | 0.27 |
| **b) Comparison with CNRM - RCSM6 Hindcast Run (1982-2014)** | | | | | |
| **CNRM-RCSM6 (HIST)** | **Corr.Coeff** | 0.68 | 0.69 | 0.92 | 0.74 |
| | **RMSE (days)** | 0.27 | 0.24 | 0.20 | 0.21 |

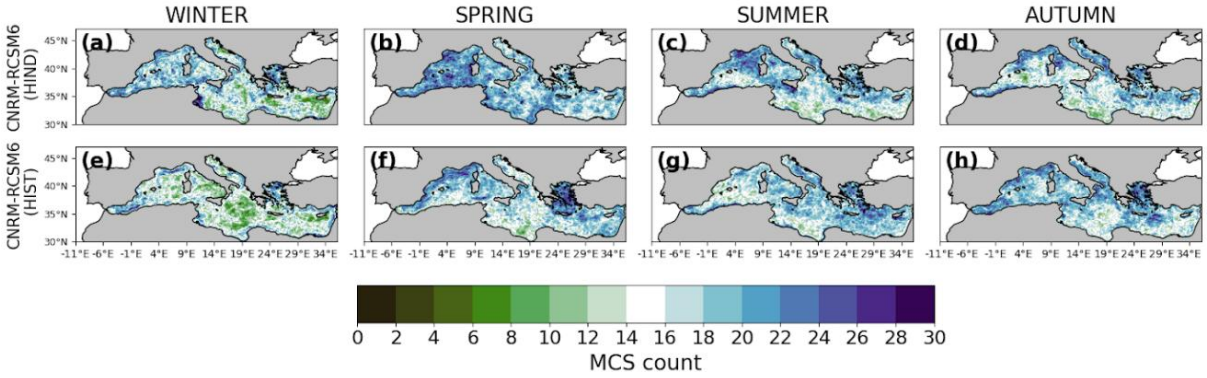


**Figure S1:** Total number of historical, MLT-based MCSs in the Mediterranean Sea across seasons throughout 1980-2017. The total number of events is shown locally for winter (DJF), spring (MAM), summer (JJA) and autumn (SON). Row

corresponds to events detected in a-d) CNRM-RCSM6 hindcast, and e–h) CNRM-RCSM6 historical simulations. MCSs were identified by applying Hobday et al. (2016) MLT from the historical simulation (1980–2014) and the hindcast run (1982–2017), with 1982–2014 used as the baseline climatology. Seasons are assigned based on the MCS onset date, regardless of termination.

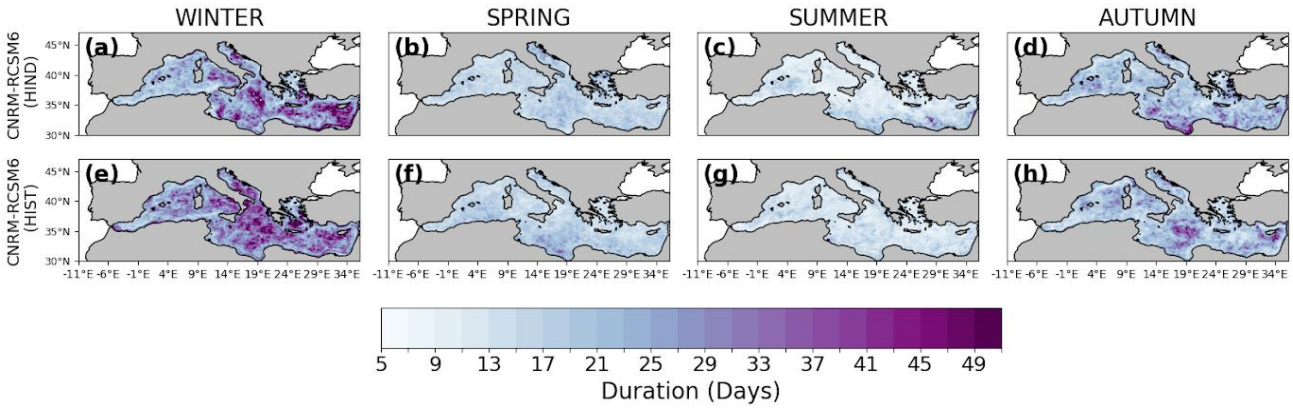


**Figure S2**: As in Figure A1 but for mean duration of MCS based on MLT.

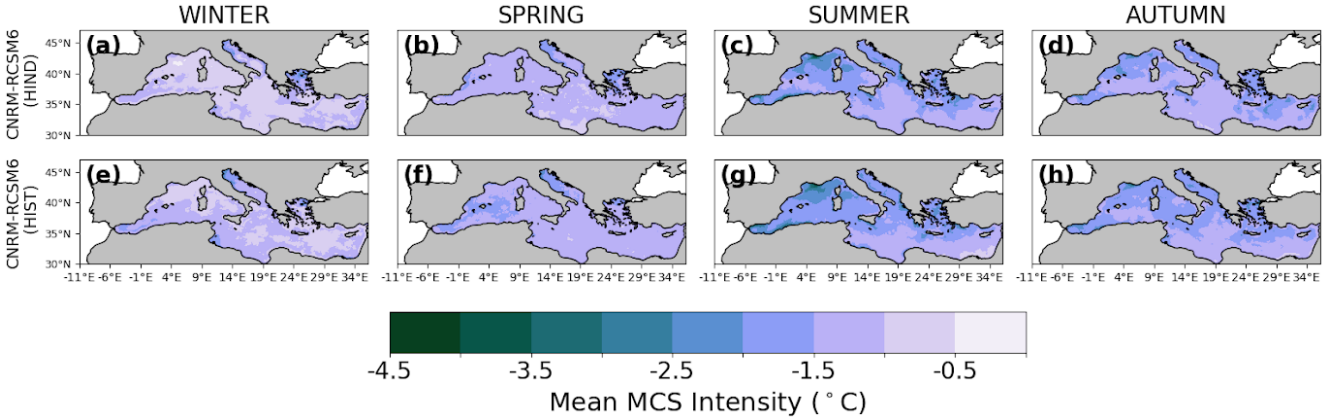


**Figure S3:** As in Figure A2 but for mean intensity of MCS based on MLT**.**

**Table S5:** Basin-mean MCS count, duration and intensity based on MLT of the CNRM-RCSM6 hindcast (1982–2017) and historical run (1980–2014) periods. The corresponding Pearson product-moment correlation coefficient and root mean square error (RMSE) are also shown for the two simulations in different seasons. MCS were identified by applying the Hobday et al. (2016) framework on MLT and seasons are defined based on MCS onset dates, with no constraint on the termination season.

| MCS property | Dataset | Winter | Spring | Summer | Autumn |
|---|---|---|---|---|---|
| Total MCS Count | CNRM-RCSM6 hindcast run | 15 | 18 | 16 | 15 |
| | CRNM-RCSM6 historical run | 13 | 16 | 16 | 17 |
| | Pearson Corr.Coeff | 0.4 | 0.05 | 0.3 | 0.3 |
| | RMSE | 4.9 | 4.8 | 4 | 4.2 |
| Duration (days) | CNRM-RCSM6 hindcast run | 22 | 15 | 12 | 18 |
| | CRNM-RCSM6 historical run | 25 | 15 | 12 | 18 |
| | Pearson Corr.Coeff | 0.39 | 0.16 | 0.31 | 0.26 |
| | RMSE | 9.3 | 3.8 | 3.6 | 6.5 |
| Intensity (°C) | CNRM-RCSM6 hindcast run | -1 | -1.2 | -1.7 | -1.5 |
| | CRNM-RCSM6 historical run | -1.1 | -1.4 | -1.7 | -1.6 |
| | Pearson Corr.Coeff | 0.7 | 0.6 | 0.9 | 0.7 |
| | RMSE | 0.2 | 0.2 | 0.2 | 0.2 |

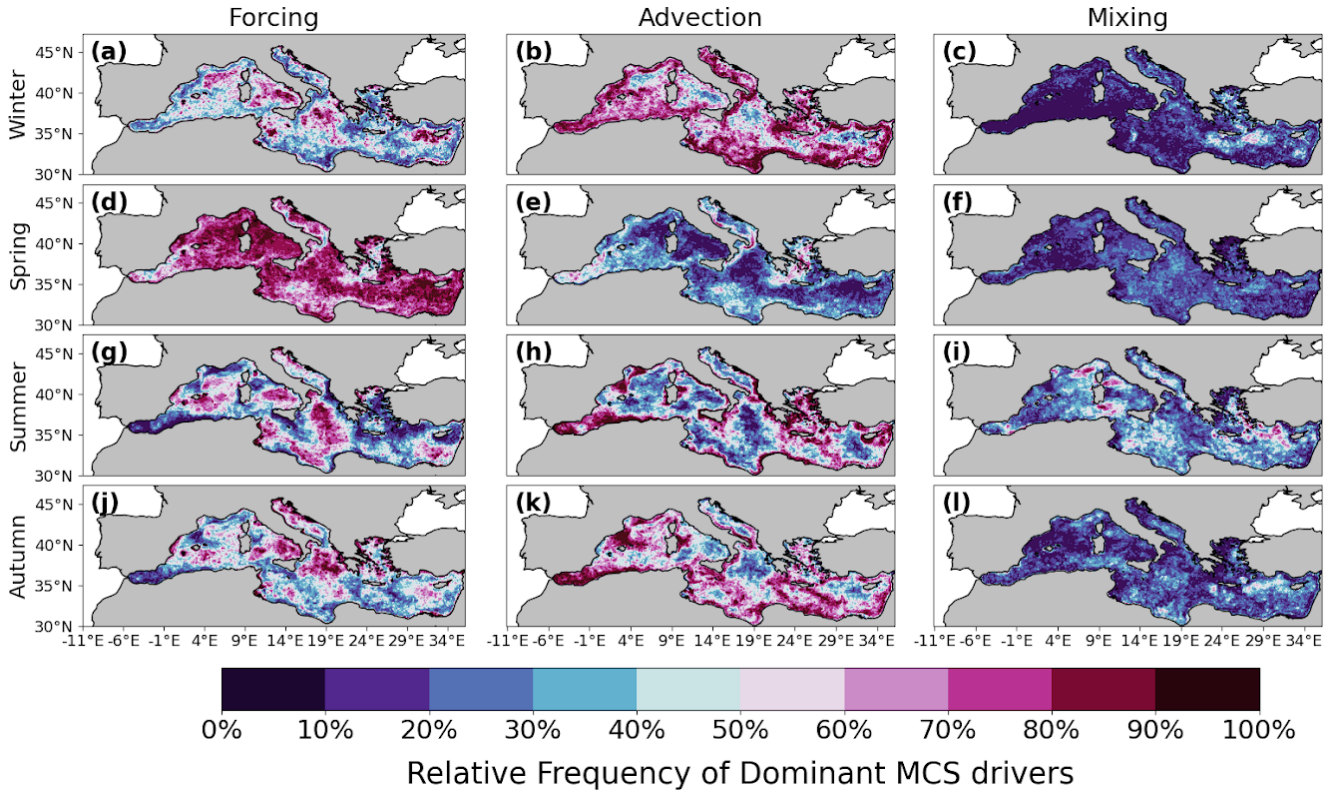


**Fig.S4:** Seasonality of dominant drivers of Mediterranean MCS onsets in the CNRM-RCSM6 hindcast simulation (1982–2017), based on MLT. At each grid point, percentage represents the number of MCS onsets attributed to each MLHB process (columns), relative to the total number of identified onsets during the examined period, in each season (rows). Seasonal classification is based on the date of MCS onset, with no constraint on the termination season. The events were identified based on the model's MLT, with a baseline period of 1982-2014.

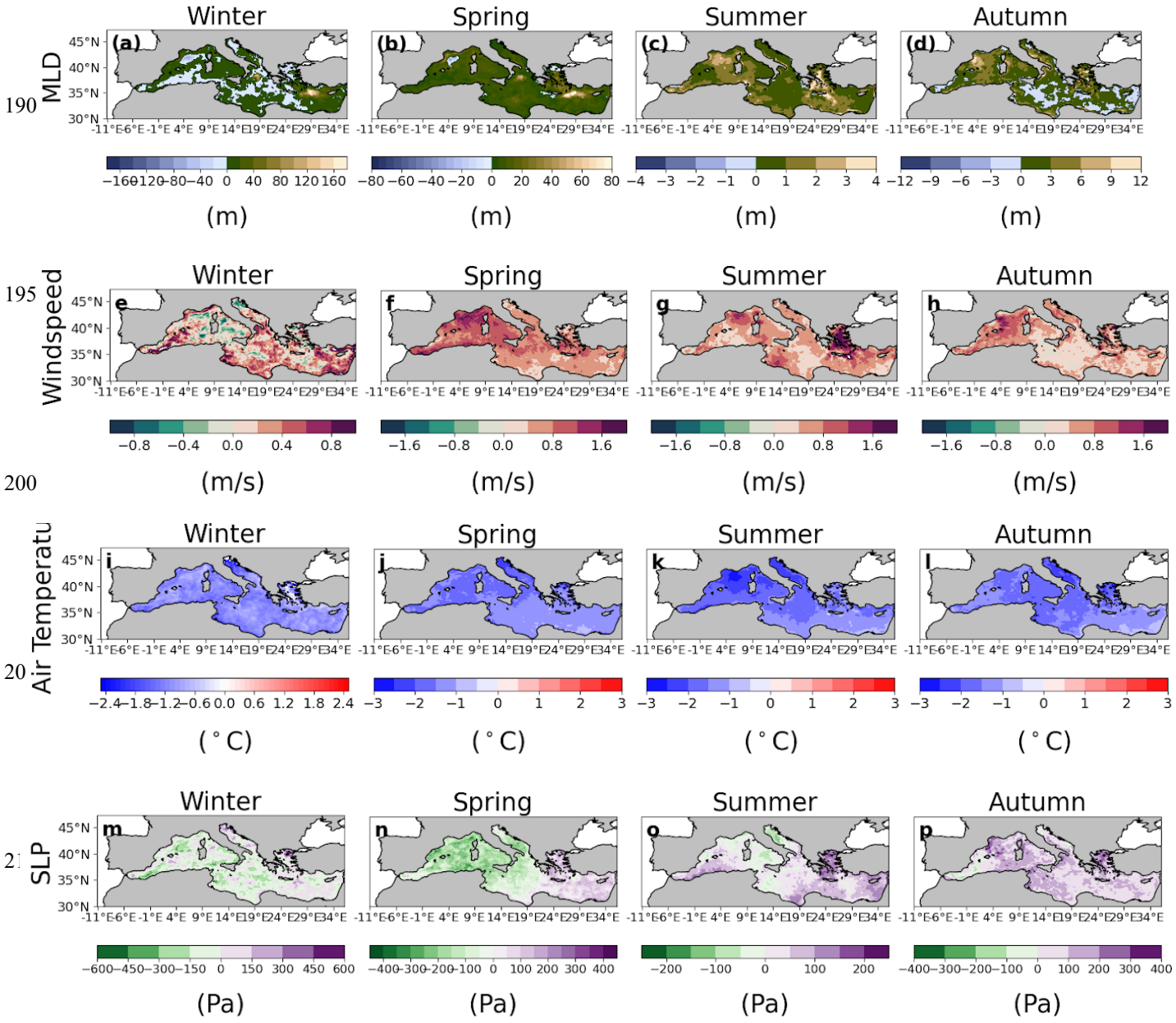


**Fig.S5**: Composite anomalies of MLD (a-d), wind speed (e-h), 2m-air temperature (i-l) and sea level pressure (m-p) relative to the climatology (1982-2014), calculated over the duration of MCSs. At each grid point anomalies are averaged across all MCS events during the period 1982–2014. Columns correspond to winter (DJF), spring (MAM), summer (JJA), and autumn (SON). Daily variables were obtained from the coupled ALADIN-climate atmospheric model at 12 km resolution (Sevault et al., 2014) for the period 1982–2014. MCSs are identified by applying the Hobday et al. (2016) framework to simulated daily

mixed layer temperature (MLT) over the same period. Seasonal classification is determined by the date of MCS onset, irrespective of termination. For each grid point, anomalies in all variables are computed over the start and end dates of the MCS events identified at that location.

**Table S6**: Basin-mean, MCS count, duration and intensity during events in GWL1, GWL2 and GWL3 under the SSP5-8.5 simulation of CNRM-RCSM6. MCSs are identified based on MLT and relative to a fixed baseline in the past (1982-2014). Seasonal classification is based on the date of MHW onset, with no constraint on the termination season. MCS drivers are not assessed at GWL4, as conditions at this warming level exceed the thermal thresholds required for their occurrence across the basin.

| MCS property | Future Period | Winter | Spring | Summer | Autumn |
|---|---|---|---|---|---|
| **MCS Count** | GWL1 | 2 | 2.1 | 2.4 | 3 |
| | GWL2 | 1.4 | 1.2 | 2 | 2 |
| | GWL3 | 1.2 | 1.1 | 1.4 | 1.2 |
| **Duration (days)** | GWL1 | 11.50 | 7.84 | 10.04 | 13.52 |
| | GWL2 | 12.50 | 7.44 | 7.61 | 9.89 |
| | GWL3 | 8.53 | 9.33 | 7.75 | 10.13 |
| **Intensity** (°C) | GWL1 | -1.20 | -1.32 | -1.80 | -1.57 |
| | GWL2 | -1.31 | -1.43 | -1.91 | -1.71 |
| | GWL3 | -1.37 | -1.32 | -2.08 | -1.83 |

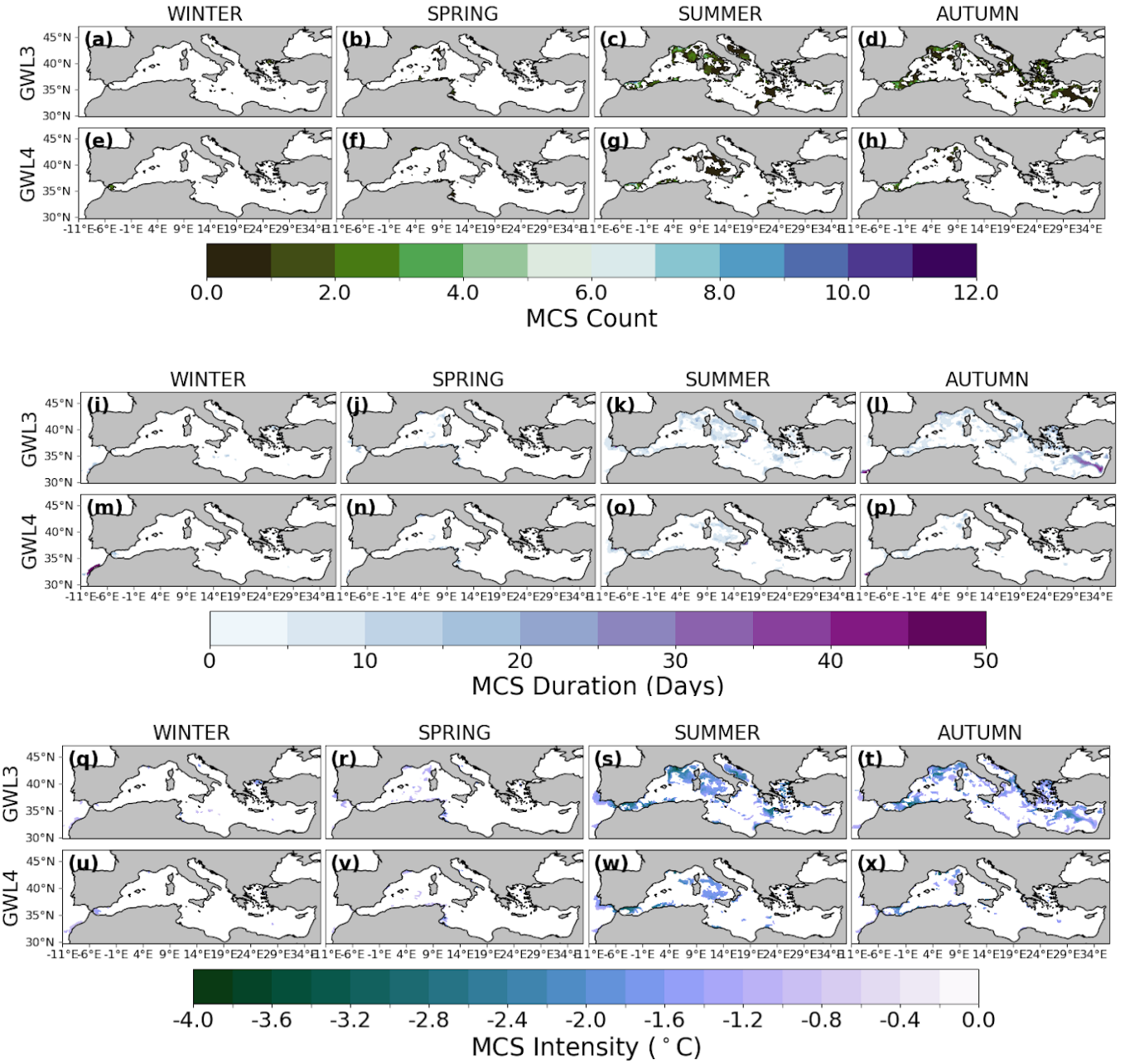


**Fig.S6:** Seasonal distribution of projected MCS count (a-h), duration (i-p) and intensity (q-x) averaged over GWL3 and GWL4. Columns correspond to winter (DJF), spring (MAM), summer (JJA), and autumn (SON) events and rows to GWL3 (2055–2074) and GWL2 (2070–2089). MCSs are identified by applying the Hobday et al. (2016) framework to simulated daily MLT under SSP5-8.5, with 1982–2014 period as the baseline climatology. Seasonal classification is based on the date

of MCS onset, regardless of termination. White areas indicate regions where MCS are not projected due to thermal exceedance preventing their occurrence.

290

**→ Future MCS with a shifted baseline climatology**

**Table S7**: Basin-mean, annual MCS frequency, duration and intensity during events in GWL1, GWL2 and GWL3 under the SSP5-8.5 simulation of CNRM-RCSM6. MCSs are identified based on MLT and relative to a shifted baseline centered at 295 each GWL period. Seasonal classification is based on the date of MHW onset, with no constraint on the termination season.

| MCS property | Future Period | Winter | Spring | Summer | Autumn |
|---|---|---|---|---|---|
| **MCS Count** | GWL1 | 9 | 13 | 10 | 10 |
| | GWL2 | 10 | 12 | 10 | 10 |
| | GWL3 | 8 | 11 | 10 | 10 |
| | GWL4 | 8 | 9 | 9 | 10 |
| **Duration (days)** | GWL1 | 23.31 | 12.52 | 11.53 | 16.89 |
| | GWL2 | 21.28 | 12.93 | 11.29 | 16.15 |
| | GWL3 | 25.13 | 14.60 | 12.38 | 18.80 |
| | GWL4 | 27.40 | 18.45 | 11.55 | 21.61 |
| **Intensity** (°C) | GWL1 | -0.93 | -1.15 | -1.63 | -1.44 |
| | GWL2 | -0.92 | -1.12 | -1.72 | -1.59 |
| | GWL3 | -1.11 | -1.28 | -1.88 | -1.70 |
| | GWL4 | -1.22 | -1.58 | -1.91 | -1.87 |

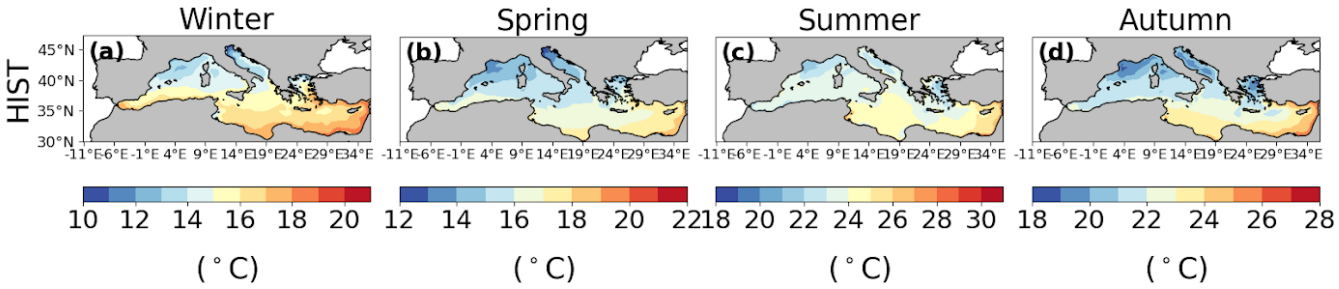


**Fig.S7**: Seasonally-averaged MLT during the historical period 1980-2014. The climatology is computed from daily MLT fields of the historical simulation following the Hobday et al. (2016) framework and using 1982–2014 as the reference climatological period. Winter (DJF), Spring (FMA), Summer (JJA), Autumn (SON).

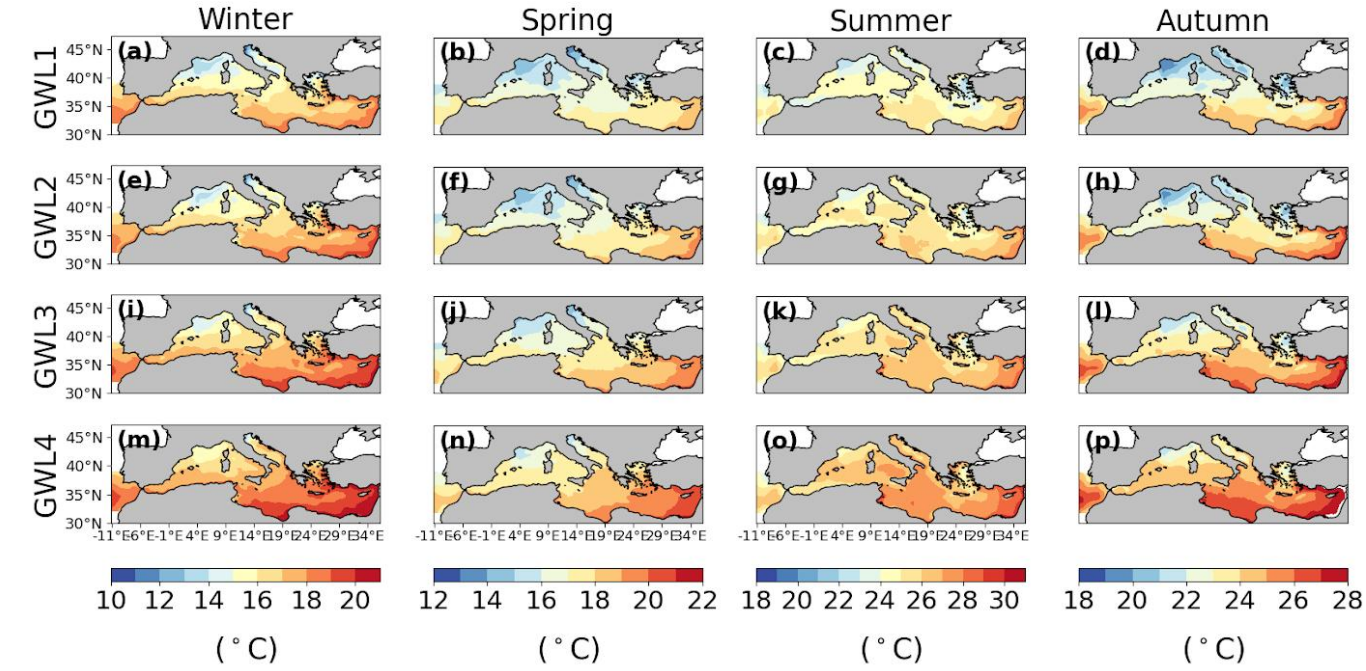


**Fig.S8**: Seasonally-averaged MLT during the future GWL1-GWL4 periods (see Table S1). The climatology was computed from daily MLT of the SSP58.5 scenario run, by applying the Hobday et al. (2016) separately to each GWL period. Climatology was centered in each GWl period Winter (DJF), Spring (FMA), Summer (JJA), Autumn (SON).

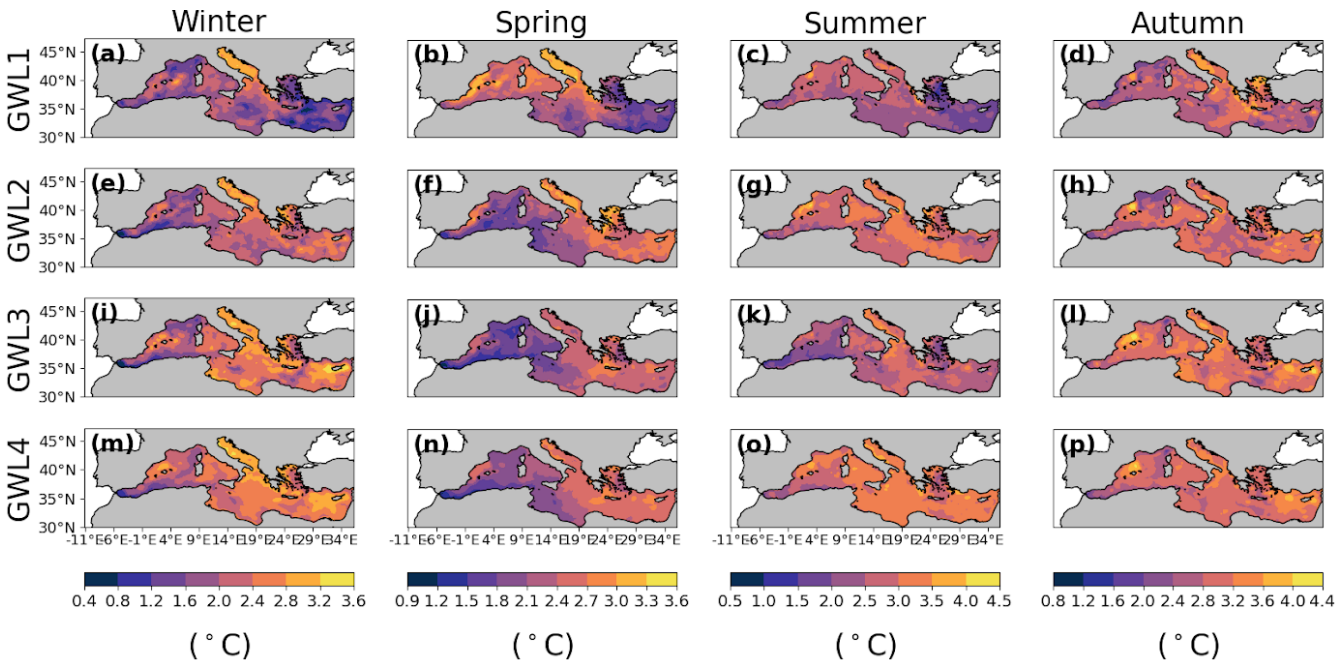


**Fig.S9**: Seasonally averaged MLT anomalies for the GWL1–GWL4 relative to the historical climatology (see Table S1). Figure S8 shows the difference between the future MLT climatologies of each GWL in Fig.S7 and the historical climatology in Fig.S6. Winter (DJF), Spring (FMA), Summer (JJA), Autumn (SON).

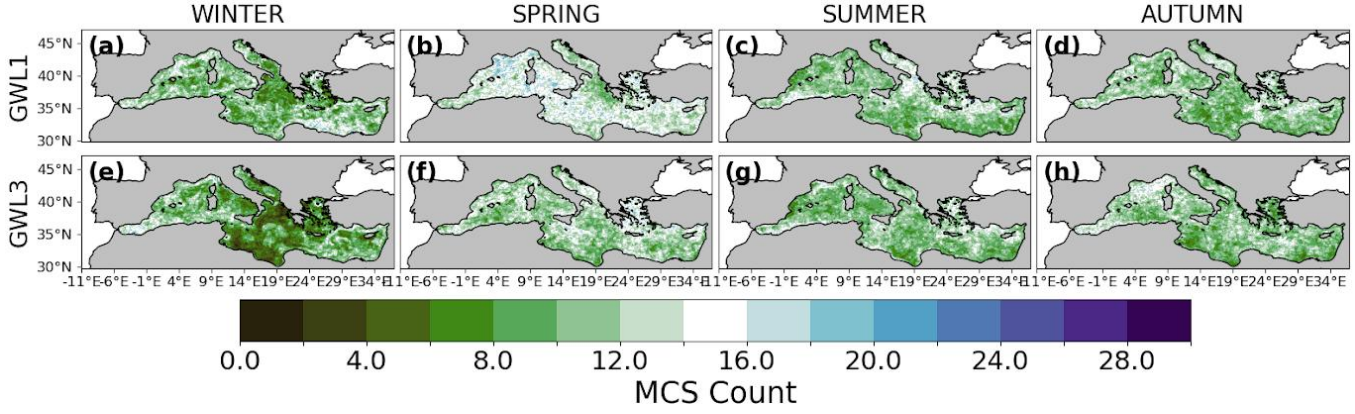

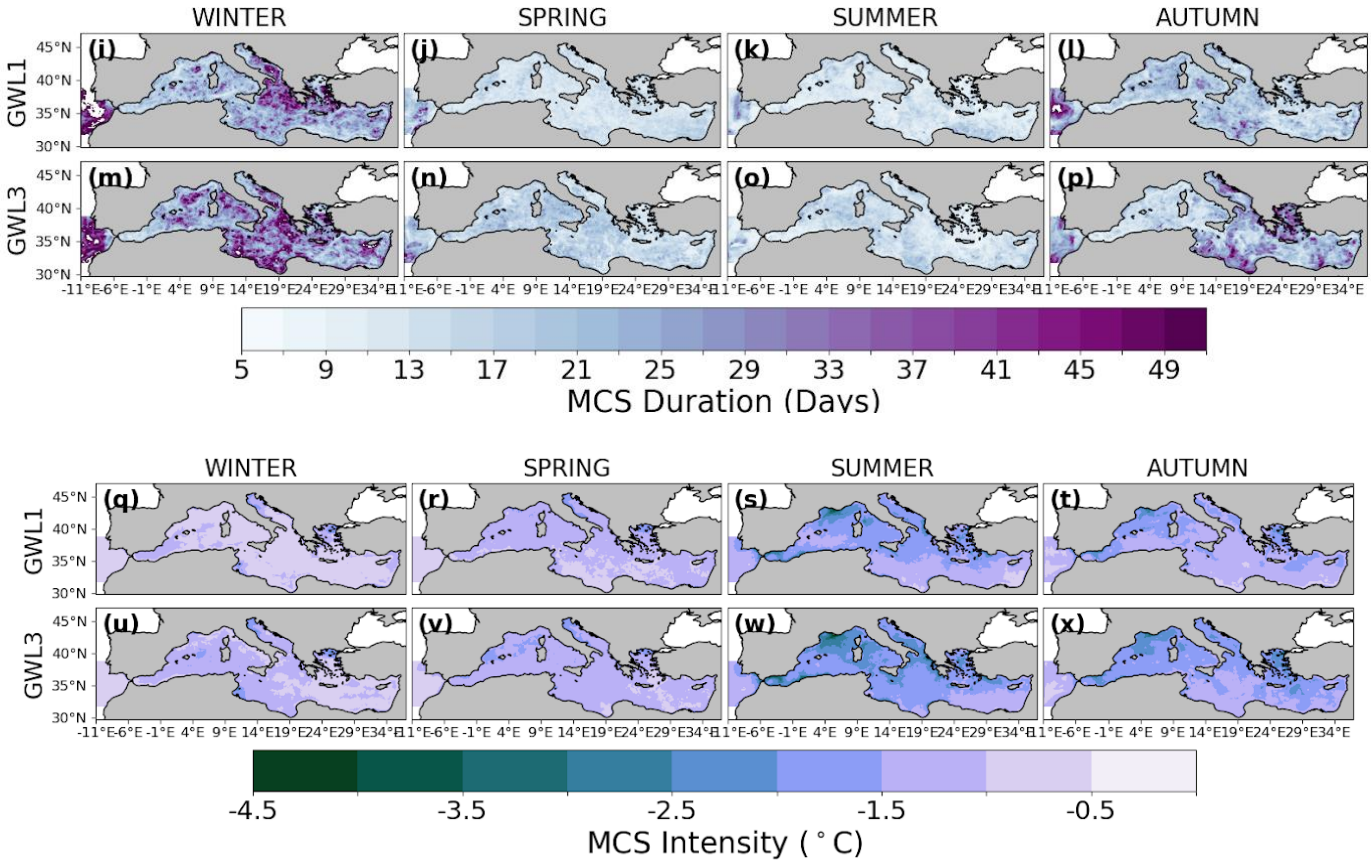


**Fig.S10:** Seasonal distribution of projected MCS count (a–h), duration (i–p), and intensity (q–x). Columns correspond to winter (DJF), spring (MAM), summer (JJA), and autumn (SON), while rows show results for GWL1 and GWL3 periods. MCSs are identified by applying the Hobday et al. (2016) framework on simulated daily MLT under the SSP5-8.5 scenario, with baseline climatologies defined for each GWL. Seasons are assigned based on the date of MCS onset.

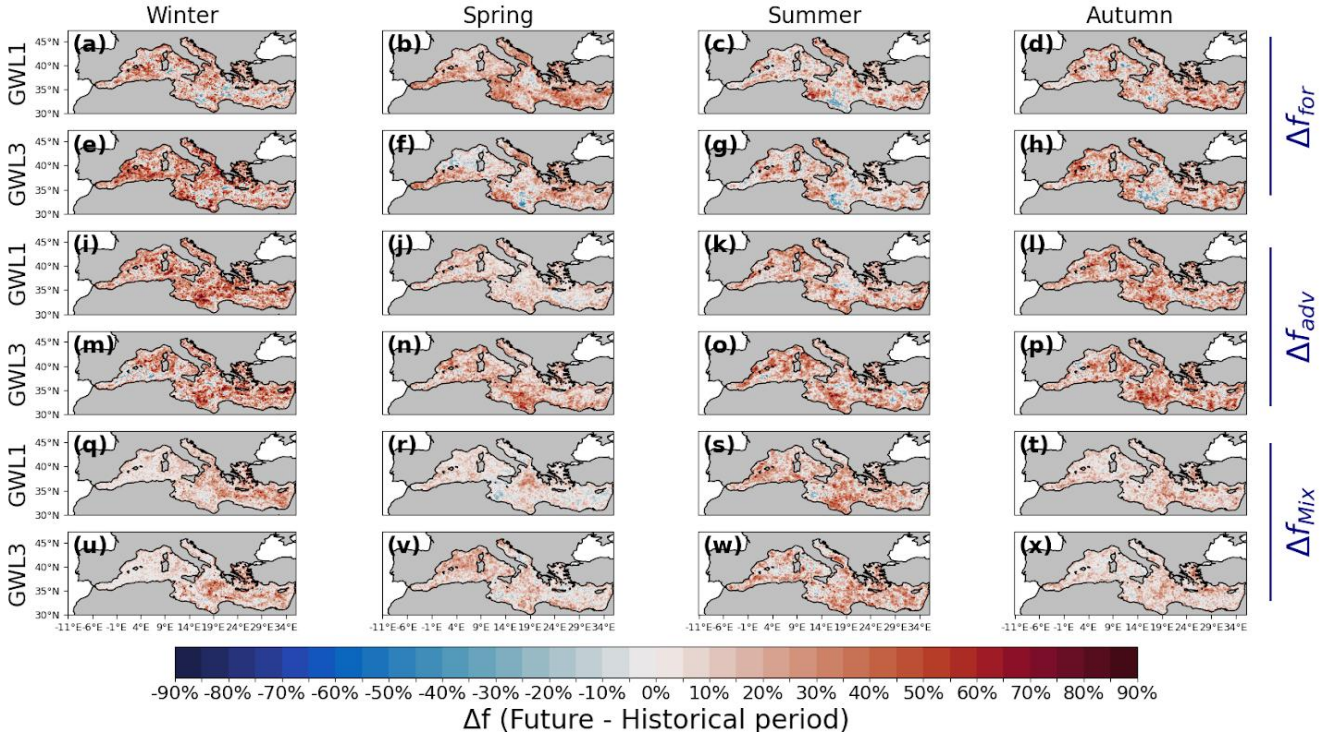


**Fig.S11**: Difference in the normalized MCS frequency between future ffuture and historical period fhist, for events dominated by Forcing ($\Delta f_{for}$; a-h), Advection ($\Delta f_{adv}$;j-p) and Mixing processes ($\Delta f_{mix}$;q-x). Based on their date of initiation, MCSs are grouped in winter (a,e,i,m,q,u), spring (b,f,j,n,r,y), summer (c,g,k,o,s,w) and autumn (d,h,l,p,t,x) and by warming levels GWL1 and GWL3 (in rows). The MCSs and their dominant drivers have been calculated relative to each GWL period (see Table S1).

435

440

445

450

455